Bioelectrochemistry 115 (2017) 33–40

Contents lists available at ScienceDirect

Bioelectrochemistry

Impedance spectroscopy as an indicator for successful *in vivo* electric field mediated gene delivery in a murine model

Reginald M. Atkins[a], Timothy J. Fawcett[a,b,c,*], Richard Gilbert[a,c], Andrew M. Hoff[c,d], Richard Connolly[a,c], Douglas W. Brown[e], Anthony J. Llewellyn[a,c], Mark J. Jaroszeski[a,c]

[a]*Department of Chemical and Biomedical Engineering, University of South Florida, 4202 E. Fowler Ave. ENB 118, Tampa, FL 33620, USA*
[b]*Research Computing, University of South Florida, 4202 E. Fowler Ave. ENB 118, Tampa, FL 33620, USA*
[c]*Center for Molecular Delivery at USF, University of South Florida, 4202 E. Fowler Ave. ENB 118, Tampa, FL 33620, USA*
[d]*Department of Electrical Engineering, University of South Florida, 4202 E. Fowler Ave. ENB 118, Tampa, FL 33620, USA*
[e]*School of Electrical and Computer Engineering, Georgia Institute of Technology, 777 Atlantic Dr. NW, Atlanta, GA 30332, USA*

ARTICLE INFO

Article history:
Received 3 March 2016
Received in revised form 20 January 2017
Accepted 22 January 2017
Available online 27 January 2017

Keywords:
Impedance spectroscopy
Electroporation

ABSTRACT

In vivo gene electro transfer technology has been very successful both in animal models and in clinical trials over the past 20 years. However, variable transfection efficiencies can produce inconsistent outcomes. This can be due to differences in tissue architecture and/or chemical composition which may effectively create unique biological environments from subject to subject that may respond differently to the identical electric pulses. This study investigates the integration of impedance spectroscopy into the gene electro transfer process to measure murine skin impedance spectra before, during (after pulse delivery), and after gene electro transfer pulse application to determine if changes in impedance correlate with reporter gene expression. Both post-treatment impedance spectra and gene expression were dependent upon the applied electric field strength. These results indicate that alterations in tissue impedance produced by the applied electric field represent an excellent parameter to predict degrees of transfection and gene expression. These results could ultimately be used to alter pulsing parameters in order to optimize delivery/expression.

1. Introduction

The origin of pathologies associated with aberrant genes has been studied extensively [1–6]. It is now accepted that both inherited and acquired genetic mutations are culpable for many chronic diseases. Technologies with the ability to deliver correctly sequenced genes encoding properly functioning proteins into cells provide an excellent opportunity for the treatment of pathologies caused by DNA mutations that produce absent or non-functioning proteins. However, delivering nucleic acids through cell membranes poses a challenge. Nucleic acid constructs, such as plasmid DNA (pDNA) and small interfering RNA (siRNA), are orders of magnitude larger than most drugs and possess copious negative charge making the translocation of extracellular nucleic acids across the plasma membrane unlikely under normal conditions [7,8]. To this point, a great demand exists for technology to address this obstacle if medicine is to harness the advantages of gene-based therapies.

An electric field mediated gene delivery method referred to as gene electro transfer (GET) has emerged as a formidable technique allowing for the potential of gene-based therapies to be realized. During GET, it is proposed that electric field pulses temporarily permeabilize the cell membrane facilitating exogenous DNA uptake [9]. Recently, impedance spectroscopy has been utilized the characterize the electrical properties of biological tissue [10–12]. Changes in tissue and/or cell impedance may indicate changes in the membrane permeability induced by GET [9,13-15]. This work supports the integration of impedance spectroscopy into GET methods as a way to significantly enhance the probability that gene delivery occurs by optimizing the number of electric field pulses to target optimum membrane permeability. Real time use of tissue impedance measurements can be used to decide whether more electric field pulses are required to maximize gene delivery. In order to it validate the potential of this method it is necessary to juxtapose/assess the efficacy of GET with other methods that have contributed to gene delivery/therapy research.

An array of technologies exist for enhancing the intracellular delivery of nucleic acids broadly classified as either viral or non-viral methods. Viral methods employ live viruses to transfect host cells

* Corresponding author.
E-mail address: tfawcett@usf.edu (T.J. Fawcett).

http://dx.doi.org/10.1016/j.bioelechem.2017.01.004
1567-5394/

with a gene of interest. This is accomplished with great efficiency but also with safety concerns. Many viral vectors randomly integrate their genome into the host genome increasing the risk for insertional mutagenesis and subsequent malignant transformation [16]. Other viral vectors target specific regions of the host genome for integration but with a limited payload capacity for exogenous nucleic acids [17–19]. Although effective, viral vectors raise safety concerns associated with their immunogenicity. Natural exposure to viruses over time engenders immunity to their components. These same viruses often induce immune responses when used to deliver genes [20,21].

Non-viral methods utilize physical or chemical processes to induce gene delivery. Chemical methods that use liposomes and cationic surfactants that encapsulate pDNA exhibit relatively lower transfection efficiencies and cell viability [22,23] compared to viral methods. Chemical methods often involve a systemic distribution of therapeutics that may lead to unwanted gene expression in untargeted cells [24]. There are a collection of different methods for delivering pDNA including single cell laser cutting [25], mechanical perturbation via ultrasonic treatment [26,27], biolistic transfection (gene gun) [28], magnetic fields [29], and electric fields [30–32]. Unlike chemical methods, physical methods do not require exposure to chemicals. Physical and chemical methods produce transient transfection only with periodic treatments required to maintain high expression levels of the encoded protein.

Gene electro transfer, the application of electric fields to tissue, represents a physical method that relies upon the membrane permeabilizing effect of electric pulses/fields [9,33-39]. When a specific electric field is employed to deliver genes, extracellular nucleic acids pass through the membrane via a mechanism that is not clearly understood [40,41]. These genetic constructs translocate to the nucleus where the gene expression process begins. Permeabilizing electric fields are established by applicators containing electrodes in direct contact with the target tissue. Typical electrode spacing requires the delivery of electrical pulses on the order of tens of volts for hundreds of milliseconds to attain field strengths between 100 V/cm and 200 V/cm [42,43]. These electric fields generated in the skin cause ions in the local extracellular space and within cells to collect on the inner and outer leaflets of cell membranes similar to the charging of a capacitor [44]. As the ions accumulate, the transmembrane potential eventually reaches a breakdown voltage of the insulating phospholipid bilayer resulting in current flow through the membrane and permeabilization [45,46]. Rearrangements in cell membrane structure following permeabilization provide new pathways for current resulting in measurable changes in electrical conductivity. Changes in conductivity can therefore be used to indicate when changes in membrane permeability occur [47–50]. Such changes in tissue conductivity and capacitance allow impedance spectroscopy to be used as a tool for quantifying changes in the electrical characteristics of cells/tissue as a result of gene electro transfer [9,10,12-15,47,51-53].

Current *in vivo* electro transfer treatment protocols typically apply a fixed set of pulses to the tissue to obtain gene delivery. The pulse characteristics (field strength, pulse duration, number of pulses, etc.) are typically empirically derived based upon mean responses from preclinical studies. When determining these optimal parameters, there is currently no method available to account for differences between individuals with respect to chemical environment and tissue architecture. Similarly, empirical approaches do not permit the ability of real time alterations of pulse parameters in response to any measured parameter (such as impedance or conductivity changes in the tissue) during electrical treatment nor do they provide any indication of successful gene delivery. Thus, any differences in chemical environment and/or tissue architecture will result in large variations in gene delivery thereby decreasing the reliability and clinical relevance of this gene delivery method. Although gene electro transfer has been successful and will likely have many applications in the near future, it is likely that it can be ultimately improved by measuring changes in electrical properties during gene electro transfer. This paper reports on research efforts to identify impedance spectra characteristics of tissue that correlate with successful gene delivery.

2. Methods

2.1. Hardware

The electric field delivery instrumentation hardware includes thirty-two (32) isolated solid state relays within a single National Instruments (NI) SCXI-1163R module housed in a NI SCXI-1000 chassis. The module is controlled by an NI SCXI-1600 USB Data Acquisition and Control Module (200 kS/s). Sixteen of the relays were connected to the positive terminal while the other sixteen relays were connected to the ground terminal of a high voltage power supply (Glassman High Voltage Inc., PS/EW02R300-115). Impedance spectroscope was created from a National Instruments (NI) USB-6361 multifunction input/output card that generated a multi-frequency sine analog voltage reference signal buffered by a unity gain high-bandwidth amplifier (Linear Technology LT1358) rated to drive capacitive loads. The differential voltage across and current flowing through the tissue was buffered (LT1359) and measured by a pair of instrumentation amplifiers (LT1995) before being recorded by the analog input channels of the USB-6361. The sampling rate for both the reference signal generation and voltage/current measurements was 1 MHz. The electric field generation and impedance measurement instrumentation were combined into a single composite instrument system that permitted impedance spectra to be obtained before and/or after electric field pulses were applied using the same electrode array. This arrangement assured that the electric field and the impedance measurement occurred in the same tissue region. This was achieved through the use of a series of high-voltage reed relays (Cynergy3 DAT71210) that were used to rapidly connect/disconnect the high voltage pulse delivery instrument and the low voltage impedance measurement portion of the instrument. All devices were connected to a laptop computer and controlled via a custom NI Labview 2013 application.

2.2. Applicator and pulsing sequences

Pulsed electric fields were applied and impedance measurements were made using a direct contact multielectrode array (MEA) applicator, shown in Fig. 1A, constructed with sixteen gold-plated 0.54 mm diameter flat bottom electrodes (100039-025-958, Interconnect Devices). The electrodes were spaced 2.5 mm apart center to center creating a square geometry with a side length of 8.0 mm. This array created nine 2.5 mm by 2.5 mm square spaces between electrodes with each spacing referred to a sector of treated tissue. Each electrode in this MEA applicator was spring loaded which allowed the tips to conform to differences in animal skin topology ensuring electrodes were in good contact with tissue [21,42,43].

Treated animals received DC pulses 150 ms in duration with a 500 ms interval between pulses. Fig. 1B shows a schematic of electrode placement on the skin of the animal and also numerically identifies each electrode (1–16) and sector (S1–S9). Electric pulsing and post-pulse impedance measurements were conducted in each sector sequentially (S1 through S9). For example, the first pulsing sequence was executed in sector 1 (S1) with the following pattern: four pulses with electrodes 1 and 5 positive potential and electrodes 2 and 6 ground. Next, four pulses were applied with electrodes 1 and 2 positive and electrodes 5 and 6 ground. Immediately after pulsing S1, impedance measurements were made in this sector using the same horizontal then vertical sequence as was used for pulsing.

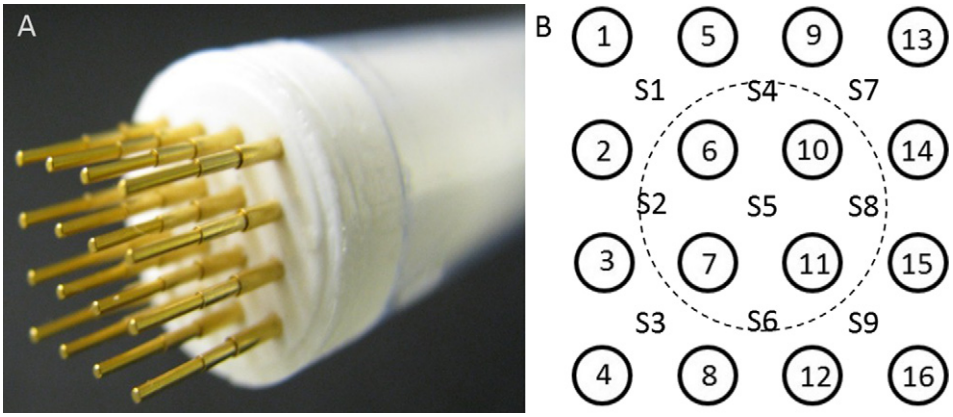

Fig. 1. (A) Image of multielectrode array, (B) schematic of electrodes (1–16) with sector labels (S1–S9) numbering sets of 4 electrodes. Dashed line is an indicator of the approximate relative size of the intradermally injected bolus of DNA centered around electrodes 6, 7, 10, and 11.

Then, the system moved to sector 2 (S2) to start the eight pulses in this sector followed by impedance measurements. Each subsequent sector, S3–S9, was treated in the same manner. Impedance was measured for all sectors (both horizontally and vertically) immediately before the first voltage pulse in S1 to provide prepulsed values for comparison.

2.3. Impedance measurement

As indicated above, the MEA applicator was used for both the application of electric fields for gene electro transfer and for impedance measurements. The impedance spectroscope generated a 1 V amplitude continuous sine wave excitation signal containing linearly spaced frequencies from 10 Hz to 100 kHz with a total duration of 25 ms. This 25 ms duration signal began 50 ms after the eighth (last) pulse in each sector. Once the voltage and current waveforms were collected, the Fourier transform of both waveforms was calculated using the Fast Fourier Transform (FFT) algorithm with a rectangle window implemented in NI Labview 2013 expressed as frequency dependent complex numbers ($\mathscr{F}_V(\omega)$ and $\mathscr{F}_I(\omega)$ respectively). The magnitude of the impedance $|Z(\omega)|$ was calculated as the ratio of magnitudes of $\mathscr{F}_V(\omega)$ relative to $\mathscr{F}_I(\omega)$ while the phase of the impedance (ϕ_Z) was calculated as the phase of $\mathscr{F}_V(\omega)$ (ϕ_V) relative to $\mathscr{F}_I(\omega)$ (ϕ_I). Prior to any animal impedance spectroscopy measurements, the impedance spectrum of the MEA applicator electrodes were shorted and impedance measurements acquired for all sectors. The contribution to the instrumentation spectra for each sector was then subtracted from all subsequent spectra obtained from tissue.

2.4. Treatment

Mixed sex BALB/c mice (Charles Rivers) 8–10 weeks of age were used for this study. The right flank of each animal was shaved 48 h prior to DNA delivery using standard animal clippers. Immediately before treatment, animals were anesthetized in an induction chamber that was continuously supplied with a 2.5% isofluorane/97.5% oxygen mixture (Caliper Life Sciences). Once anesthetized, individual animals were removed from the induction chamber and kept anesthetized under the same 2.5% isofluorane in oxygen mixture attached to a standard scavanged rodent nose cone. Also, animals rested on a warming pad to maintain body temperature during delivery procedures.

Nine different animal treatment groups were established to evaluate both the utility of impedance data for predicting the enhanced delivery of luciferase plasmid to murine skin and the impact the low voltage impedance measurement process had on delivery. One treatment group was an untreated control group which received neither an applied electric field treatment nor a pDNA injection. A second group received pDNA only (DO). Five treatment groups received pDNA followed by electric pulses and also had impedance measurements taken before, during and after electrical treatment (DEI). These 5 groups varied only in the applied electric fields which were 50 V/cm, 100 V/cm, 150 V/cm, 200 V/cm and 250 V/cm. The remaining two groups received pDNA and electric pulses (DE) and did not have impedance measurements taken. These received electric fields of 150 V/cm and 200 V/cm. DNA was administered intradermally as a bolus injection by a 1 cm^3 syringe and 30 gauge needle (BD). Each injection contained 50 μL of gWiz Luciferase pDNA (Aldevron) at a concentration of 2 mg/mL, resulting in a total of 100 μg/injection.

2.5. Biological response, quantification, and statistical analysis

Expression was quantified from luminescence produced by the oxidation of luciferin by the expressed reporter gene luciferase. Each animal was anaesthetized, as describe above, and given a 200 μL intraperitoneal injection of D-luciferin at 15 mg/mL (Gold Biotechnology Inc.). Animals, remained anaesthetized for 15 min to allow luciferin to diffuse to the treatment site and provide enough time for luciferin luminescence to reach a maximum. Animals were then placed into a Xenogen IVIS 200 series imaging system (Caliper Life Sciences) and radiance (photons/s) was measured over a 10 second exposure time. This procedure was used to collect luminescence data at 2, 4, 7, 10, 14 and 30 days post-treatment. Once all data was collected, the mean radiance and standard error of the means for each group at all time points were calculated. Comparison of radiance between groups to determine statistical significance was performed using a single-tailed Student's *t*-test at a 95% confidence level.

3. Results and discussion

3.1. Gene expression

Fig. 2 shows luciferase luminescence data for a representative animal for all DO (pDNA only) and DEI (pDNA, electric field pulses, and impedance measurements) groups 14 days post-treatment. Radiance of the control group that did not receive plasmid injections or exposure to electric fields was taken to determine background luminescence. As expected, pDNA expression increased with increasing field strength for fields below 250 V/cm in which the amount of expression was less than that of 100 V/cm but still greater than the DNA only animals. Measurable expression of luciferase in the DO

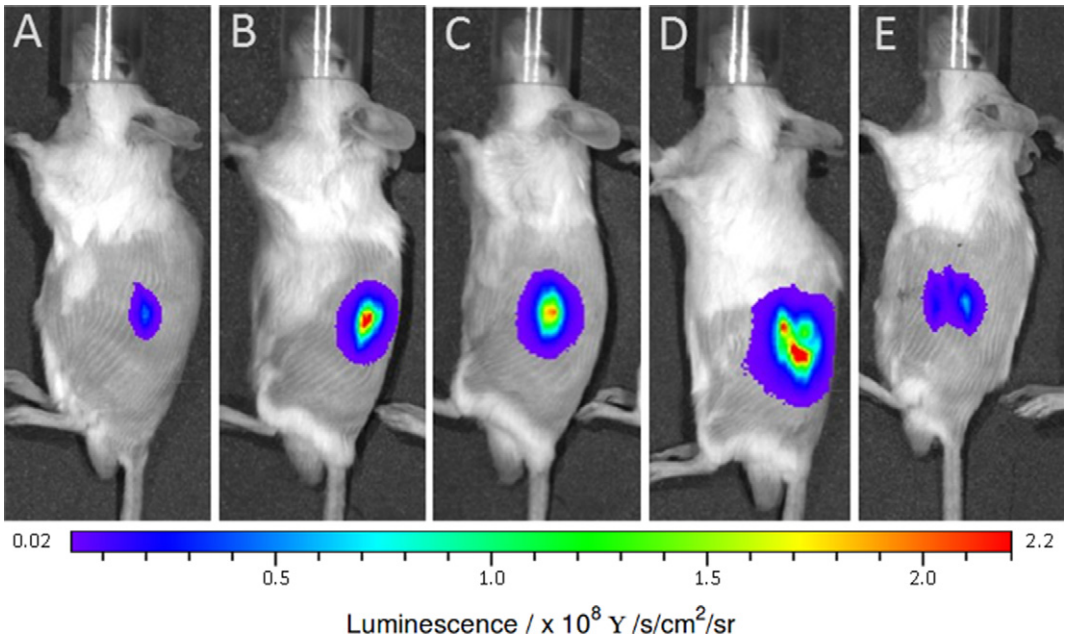

Fig. 2. Xenogen images showing luciferase luminescence at day 14 for one representative animal from each of the following groups: (A) DO group, (B) DEI-100V/cm group, (C) DEI-150V/cm group, (D) DEI-200V/cm group, and (E) DEI-250V/cm group.

group was expected as there is typically some uptake of plasmid by cells at the injection site.

Fig. 3 shows mean luciferase luminescence data for all DO and DEI groups at 2, 4, 7, 10, 14, and 30 days post-treatment. As expected, these levels remained constant throughout the duration of the experiment. Luciferase expression levels of the DO, DE (not shown), and DEI groups reached a maximum on day 14 and decayed to background levels by day 30. However, expression levels were near maximum at day 2 for all groups. Biological response (luciferase levels) generally increased as field strength increased, suggesting a greater degree of membrane permeabilization and/or DNA uptake as field strength was increased. A field of 200 V/cm produced the highest expression levels. However, skin treated with a 250 V/cm field (highest field) produced the lowest luciferase expression levels. These were above the levels of the DO group which may have indicated that a portion of cells were irreversibly permeabilized resulting in cell death. Further evidence of this was based upon macroscopically observable damage to skin including small lesions which ultimately formed scabs. Lower field strength groups had no observance tissue damage.

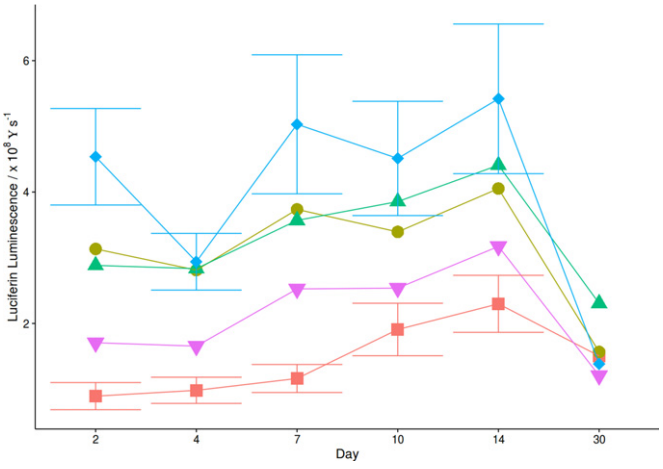

Fig. 3. Mean luciferin luminescence for all groups at 2, 4, 7, 10, 14, and 30 days post-treatment with representative error bars showing the standard error of the mean for DO groups (■) and DEI groups exposed to 100 V/cm (●), 150 V/cm (▲), 200 V/cm (♦), 250 V/cm (▼).

The radiance levels of the DEI groups where highest at day two relative to the DO group. Animals exposed to 200 V/cm had the greatest increase in expression levels as indicated by the means and associated single-tail *t*-test *p*-value presented in Table 1. The greatest relative expression levels were produced with a field strength of 200 V/cm which exhibited a 5 fold increase in mean radiance relative to DO group at day two and dropped to 2.36 fold by day 14. The relative expression levels for 100 V/cm and 150 V/cm field strengths produced relative radiance levels on day two that were 3.13 and 2.9 folds higher than DO group respectively. The 200 V/cm group had statistically higher expression levels over the DO group for 14 days post-treatment ($p = 0.0113$). The 200 V/cm group demonstrates the highest level of DNA transfection as seen in both the magnitude and duration of radiance values relative to the DO group. Impedance pulses where shown to have no statistically significant effect (*p* values greater than 0.1 at all time points in a two-tailed *t*-test) on radiance levels. This was expected as the electric fields (0.25 V/cm) generated from low voltage impedance measurements

Table 1
Mean luciferin luminescence for all groups at 2, 4, 7, 10, 14, and 30days post-treatment.

Group	Mean luciferin luminescence/$\times 10^8 \Upsilon s^{-1}$					
	Day 2	Day 4	Day 7	Day 10	Day 14	Day 30
Injection only	0.89	0.98	1.16	1.91	2.3	1.5
DEI-100 V/cm	3.13***	2.81**	3.73**	3.39*	4.05	1.57
DEI-150 V/cm	2.88***	2.83***	3.57**	3.85**	4.41**	2.31
DEI-200 V/cm	4.54***	2.94***	5.03**	4.51**	5.42*	1.39
DEI-250 V/cm	1.71*	1.65*	2.53*	2.54	3.17	1.21
DE-100 V/cm	2.17**	2.44**	2.69**	3.26*	3.58*	1.78
DE-200 V/cm	3.29***	3.37***	3.03***	3.3*	3.91*	1.37

$n = 12$ animals for all groups.
* sig. at p ¡ 0.05.
** sig. at p ¡ 0.01.
*** sig. at p ¡ 0.001.

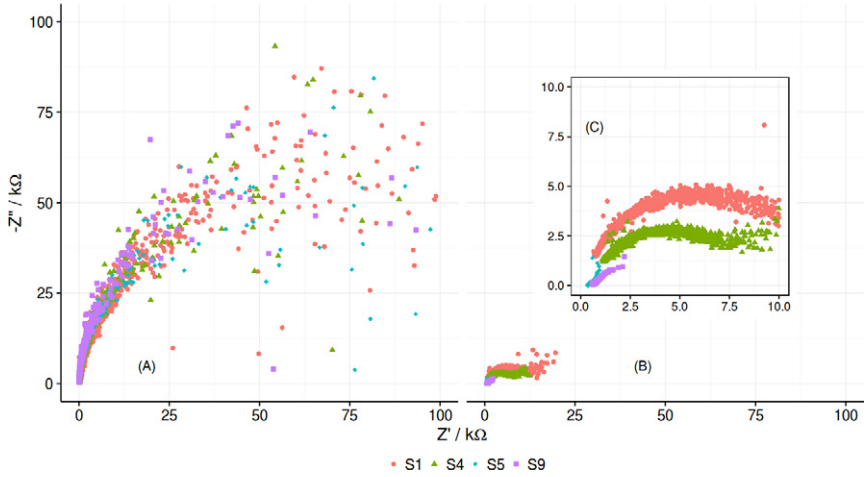

Fig. 4. Nyquist plot for a single representative animal in the 200 V/cm (A) before and (B and C) after electric field for sectors S1, S4, S5, and S9. See Fig. 1 for sector locations.

were not likely to contribute to DNA uptake. The non-intrusive, label-free nature of low voltage impedance pulses are ideal for real time electrical characterization without interfering with the biological process(es) being studied.

3.2. Impedance spectroscopy

A Nyquist plot for representative impedance measurements for several representative sectors (S1, S4, S5, and S9 of the 16 pin array, see Fig. 1) both before and after electric fields (EF) for a single animal in the 200 V/cm group is shown in Fig. 4. The before EF Nyquist curves shown in Fig. 4A exhibit the same characteristic semicircular shape indicative of a parallel RC circuit model for cell membranes [54] and only differ by minor changes in tissue electrical properties and measurement noise. The after EF Nyquist curves shown in Fig. 4B show a dramatic decrease in the magnitude and shape of impedance relative to skin that had not yet been treated with electric pulses. In addition, the after EF Nyquist curves shown in Fig. 4C are dramatically different between each sector with sector S1 showing the smallest change in impedance and sectors S5 and S9 showing the largest changes in impedance behavior. The Nyquist curves for sectors S1 (top-left sector, first to be receive EF) and S4 (top-middle sector) shown in Fig. 4C also exhibit the semicircular shape predicted from the parallel RC circuit model (as seen in the before EF curves for all sectors) but with decreased resistance and capacitance. However, the Nyquist curves for sectors S5 (central sector) and S9 (bottom-right sector, last to receive EP) show a marked deviation from the semicircular shape of a parallel RC circuit.

Fig. 5 shows the magnitude of impedance as a function of frequency for representative impedance measurements for all sectors both before and after EF for a representative animal in the 200 V/cm group. Similar to the Nyquist plots in Fig. 4, the before EF curves all follow the same shape. However, the variations in tissue impedance are more apparent such that the magnitude of impedance for sector S1 is higher than that of all other sectors for all frequencies while the impedance of all other sectors are relatively close to each other for the before EF curves. Fig. 5 shows the after EF magnitude of impedance for all sectors with sectors S1, S4, and S7 having similar

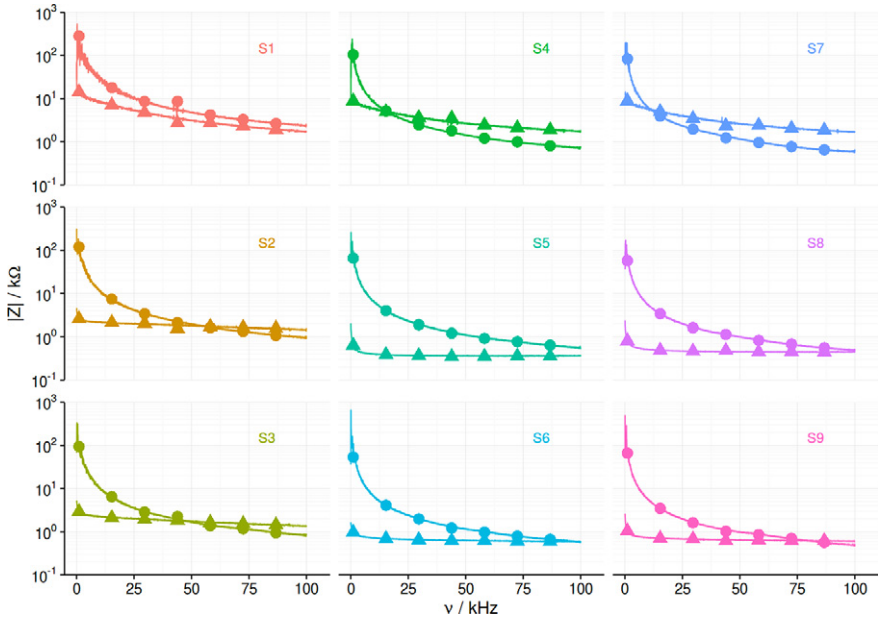

Fig. 5. Impedance magnitude versus frequency before (circles) and after (triangles) electric field for all sectors for a representative animal exposed to 200 V/cm pulses in the DEI group. See Fig. 1 for sector locations.

shape while all other sectors follow a different shape. A probable explanation for this is that effect previous electric fields generated in earlier sectors have on initiating the membrane permeabilization mechanism in cells in adjacent sectors. This may explain why sector S5 has the lowest impedance magnitude for all frequencies as sector S5 experiences the highest number of previous electric field exposures.

Comparing changes in impedance for each sector is complicated by the spatial differences in tissue impedance as seen in the before EF Nyquist curves in Fig. 4A and impedance magnitude curves in Fig. 5. To compare changes in impedance in different sectors before and after EF, the mean ratio of impedance magnitude after EF relative to before EF for DEI groups with field strengths of (A) 100 V/cm, (B) 150 V/cm, (C) 200 V/cm, and (D) 250 V/cm is shown in Fig. 6. For all field strengths shown in Fig. 6, the mean ratio of impedance after EF relative to before EF is well below 1.0 for many frequencies. The range of frequencies corresponding to mean impedance magnitude ratios less than or equal to 1.0 increased with field strength. This mean ratio being below 1.0 can be easily explained by impedance being dominated by resistance at low frequencies with the after EF resistance expected to be lower than that before EF due to new current pathways through cell membranes [47,52]. However, the mean ratio of impedance magnitude after EF relative to before EF is greater than 1.0 at high frequencies in all sectors for both 100 V/cm and 150 V/cm and several sectors in 200 V/cm and 250 V/cm. Since impedance is inversely proportional to capacitance, a mean ratio of greater than 1.0 at high frequencies may be due to the capacitance after EF being lower than the capacitance before EF.

The shape and value of the mean ratio of impedance magnitude after EF relative to before EF shown in Fig. 6 are extremely different both qualitatively and quantitatively. First, the 100 V/cm samples (Fig. 6A) had a much smaller range of frequencies in which the mean ratio was less than 1.0 than the 250 V/cm group (Fig. 6D). Second, the general shapes of the 100 V/cm curves (Fig. 6A) for each sector were overtly different than those of the 250 V/cm curves (Fig. 6D) with the exception of sectors S4 and S7. These differences may be explained by the presence of cell death in the 250 V/cm group as indicated by the reduced luciferase expression levels shown in Figs. 2 and 3 as well as observed tissue damage in these animals. However, the mean ratio curves for sectors S4 and S7 for the 250 V/cm group were similar in shape and value to those at the lower field strengths.

Fig. 6B shows the mean ratio of impedance magnitude for all frequencies after EF relative to before EF for all animals in the 150 V/cm group while Fig. 6C shows analogous data for the animals treated with 200 V/cm. The shape of the mean ratio of impedance magnitude after EF relative to before EF is similar for the 150 V/cm and 200 V/cm groups while the values for the 200 V/cm group are generally less than those of the 150 V/cm group. In addition, the range of frequencies in which the mean ratio is less than 1.0 is greater for the 200 V/cm group relative to the 150 V/cm group. These differences may be explained by increased luciferase expression levels in the 200 V/cm group relative to the 150 V/cm group indicating more successful DNA uptake as shown in Figs. 2 and 3. Differences in the shape and the range of frequencies corresponding to a mean impedance magnitude ratio less than 1.0 between sectors may be due to unequal exposure of sectors to electric fields, a result of sector spacing, pulse timing, and/or pulse sequence.

The mean ratio of impedance magnitude after electric field (EF) relative to before EF data presented in Fig. 6 cannot be directly correlated with the luciferase luminescence biological response data presented in Figs. 2 and 3 as the biological response of each sector cannot be extracted from the overall biological response due to the spatial resolution limitations of the Xenogen measurement. However, the mean overall ratio of impedance magnitude for all nine sectors and frequencies for all DEI groups (twelve animals per group) presented in Fig. 7 allows for direct comparison to the biological response data in Figs. 2 and 3. Both sets of data are measures of overall/average response throughout the entire regions of tissue affected by the gene electro transfer protocols tested. Similar to the results discussed in Fig. 6, Fig. 7 shows both the mean ratio of impedance magnitude and number of frequencies in which the ratio less than 1.0 increases with increasing field strength. Although the mechanism of DNA uptake in gene electro transfer processes and its effect on the impedance spectra of tissue after experiencing an electric field is not well understood, the mean overall ratio of impedance magnitude presented in Fig. 7 can be used as a template to generate a desired level of gene delivery when combined with the gene expression data presented in Figs. 2 and 3. For example, since the 200 V/cm group

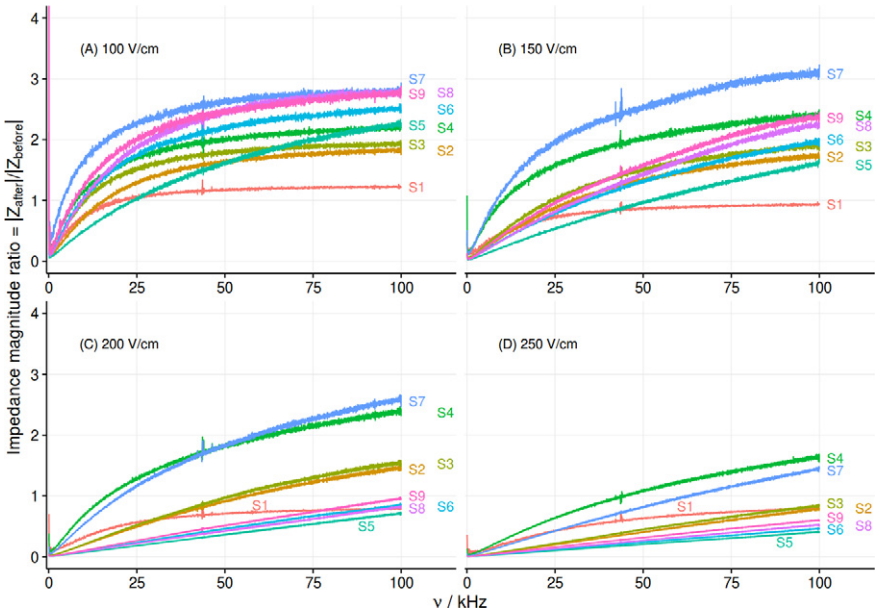

Fig. 6. Mean ratio of impedance magnitude at all frequencies after electric field relative to before electric field for DEI groups with field strengths of (A) 100 V/cm, (B) 150 V/cm, (C) 200 V/cm, and (D) 250 V/cm (twelve animals per group). See Fig. 1 for sector locations.

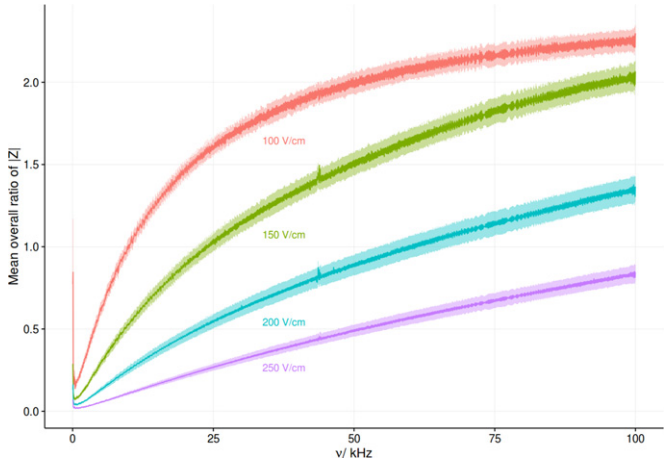

Fig. 7. Mean overall ratio of impedance magnitude over all nine sectors at all frequencies after electric field relative to before electric field for all DEI groups (twelve animals per group).

demonstrated the maximum level of gene expression in this study, the 200 V/cm mean overall impedance magnitude ratio curve presented in Fig. 7 may be used as a target to generate optimum gene expression in a four by four pulsing gene electro transfer protocol.

4. Conclusion

The current state-of-the-art for optimizing *in vivo* gene electro transfer through membrane permeabilization in different tissues has historically employed a trial and error approach. The goal of this study was to determine whether changes in tissue impedance correlate with biological responses and thus indicate successful membrane permeabilization and subsequent gene transfer. Experimental results showed a strong relationship between the change in impedance magnitude with both field strength and biological response indicating that tissue impedance is an excellent indicator of membrane permeabilization and subsequent transfection. The effect of low voltage impedance measurements before and after the application of an electric field was also evaluated to identify any significant contribution to membrane permeabilization. Considering that a 200 V/cm field strength was required to produce peak expression, it was not expected that a 0.25 V/cm impedance field would significantly increase or improve DNA uptake. Experimental results showed this to be true as there was no statistically significant difference in the biological response between DE and DEI groups of the same field strength. Results also revealed differences in the mean ratio of after electric field relative to before electric field impedance magnitudes with respect to frequency between sectors. This may be due to an unequal stimulation of sectors by electric fields from adjacent sectors and the timing in which this occurs. The distribution of impedance magnitude after EF relative to before EF versus frequency revealed interesting differences between impedance changes in different sectors underscoring the significance of pulse timing and how this relates to membrane permeabilization kinetics. A deeper examination of pore kinetics may provide insight into the pulse timing and sequence necessary for producing controlled DNA uptake in all sectors.

This research correlated identified tissue response impedance to membrane permeabilization via gene expression. Future work will identify changes in dynamic electrical parameters to be used in optimizing gene electro transfer algorithms in an attempt to target and maintain the distribution of the ratio of impedance magnitudes after EF relative to before EF versus frequency within a desired range similar to the 200 V/cm group shown in Fig. 6C. Parameters such as field strength, pulse number, frequency, and duration will be considered. This may obviate protracted trial and error methods and allow for the desired level of gene delivery obtained per application. Future efforts will also attempt to identify the impedance change that correlates with irreversible permeabilization and subsequent cell death.

Acknowledgments

The authors express our posthumous acknowledgement and sincere appreciation for Professor Anthony Llewellyn's contribution to this research. Without his wisdom and guidance, the work would still be in its infancy. His humor, knowledge, and insights are missed. Research reported in this manuscript was supported by National Institute of Arthritis and Musculoskeletal and Skin Diseases of the National Institutes of Health under award number R21AR061136. The content is solely the responsibility of the authors and does not necessarily represent the official views of the National Institutes of Health.

References

[1] E.H. Chang, J. Zabner, Precision genomic medicine in cystic fibrosis, Clin. Transl. Sci. 8 (2015) 606–610. http://dx.doi.org/10.1111/cts.12292.
[2] T. Hamidi, A.K. Singh, T. Chen, Genetic alterations of DNA methylation machinery in human diseases, Epigenomics 7 (2012) 247–265. http://dx.doi.org/10.2217/epi.14.80.
[3] H.R. Kim, S.J. Won, C. Fabian, M.G. Kang, M. Szardenings, M.G. Shin, Mitochondrial DNA aberrations and pathophysiological implications in hematopoietic diseases, chronic inflammatory diseases, and cancers, Ann. Lab. Med. 35 (2015) 1–14. http://dx.doi.org/10.3343/alm.2015.35.1.1.
[4] J.E. Trosko, C.-c. Chang, An integrative hypothesis linking cancer, diabetes and atherosclerosis: the role of mutations and epigenetic changes, Med. Hypotheses 6 (1980) 455–468. http://dx.doi.org/10.1016/0306-9877(80)90098-5.
[5] C.-A. Yang, B.-L. Chiang, Inflammasomes and human autoimmunity: a comprehensive review, J. Autoimmun. 61 (2015) 1–8. http://dx.doi.org/10.1016/j.jaut.2015.05.001.
[6] L. Zhang, E. Padron, J. Lancet, The molecular basis and clinical significance of genetic mutations identified in myelodysplastic syndromes, Leuk. Res. 39 (2015) 6–17. http://dx.doi.org/10.1016/j.leukres.2014.10.006.
[7] M.J. Meacham, K. Durvasula, L.F. Degertekin, A.G. Fedorov, Physical methods for intracellular delivery: practical aspects from laboratory use to industrial-scale processing, J. lab. autom. 19 (2014) 1–18. http://dx.doi.org/10.1177/2211068213494388.
[8] C. Rosazza, A. Buntz, T. Rieß, D. Wöll, A. Zumbusch, M.-P. Rols, Intracellular tracking of single-plasmid DNA particles after delivery by electroporation, Mol. Ther. 21 (2013) 2217–2226. http://dx.doi.org/10.1038/mt.2013.182.
[9] G. Grafström, P. Engström, L.G. Salford, B.R. Persson, 99mTc-DTPA uptake and electrical impedance measurements in verification of in vivo electropermeabilization efficiency in rat muscle, Cancer Biother. Radiopharm. 21 (2006) 623–635.
[10] D.A. Dean, T. Ramanathan, D. Machado, R. Sundararajan, Electrical impedance spectroscopy study of biological tissues, J. Electrostat. 66 (2008) 165–177. http://dx.doi.org/10.1016/j.elstat.2007.11.005.
[11] S. Laufer, A. Ivorra, V.E. Reuter, B. Rubinsky, S.B. Solomon, Electrical impedance characterization of normal and cancerous human hepatic tissue, Physiol. Meas. 31 (2006) http://dx.doi.org/10.1088/0967-3334/31/7/009.
[12] S. Laufer, S.B. Solomon, B. Rubinsky, Tissue characterization using electrical impedance spectroscopy data: a linear algebra approach, Physiol. Meas. 33 (2012) 997–1013. http://dx.doi.org/10.1088/0967-3334/33/6/997.
[13] I. Zampaglione, M. Arcuri, M. Cappelletti, G. Ciliberto, G. Perretta, A. Nicosia, N. La Monica, E. Fattori, In vivo DNA gene electro-transfer: a systematic analysis of different electrical parameters, J. Gene Med. 7 (2005) 1475–1481. http://dx.doi.org/10.1002/jgm.774.
[14] Y. Granot, A. Ivorra, E. Maor, B. Rubinsky, In vivo imaging of irreversible electroporation by means of electrical impedance tomography, Phys. Med. Biol. 54 (2009) 4927–4943. http://dx.doi.org/10.1088/0031-9155/54/16/006.
[15] R.V. Davalos, B. Rubinsky, D.M. Otten, A feasibility study for electrical impedance tomography as a means to monitor tissue electroporation for molecular medicine, IEEE Trans. Biomed. Eng. 49 (2002) 400–403. http://dx.doi.org/10.1109/10.991168.
[16] S. Hacein-Bey-Abina, C. von Kalle, M. Schmidt, F. Le Deist, N. Wulffraat, E. McIntyre, I. Radford, J.-L. Villeval, C.C. Fraser, M. Cavazzana-Calvo, A. Fischer, A serious adverse event after successful gene therapy for X-linked severe combined immunodeficiency, N. Engl. J. Med. 348 (2003) 255–256. http://dx.doi.org/10.1056/NEJM200301163480314.
[17] J. Demeulemeester, J. De Rijck, R. Gijsbers, Z. Debyser, Retroviral integration: site matters: mechanisms and consequences of retroviral integration

site selection, Bioessays 37 (2015) 1202–1214. http://dx.doi.org/10.1002/bies.201500051.
[18] C.E. Thomas, A. Ehrhardt, M.A. Kay, Progress and problems with the use of viral vectors for gene therapy, Nat. Rev. Genet. 4 (2003) 346–358. http://dx.doi.org/10.1038/nrg1066.
[19] S. de Silva, M.A. Mastrangelo, L.T. Lotta, C.A. Burris, H.J. Federoff, W.J. Bowers, Extending the transposable payload limit of Sleeping Beauty (SB) using the Herpes Simplex Virus (HSV)/SB amplicon-vector platform, Gene Ther. 17 (2010) 424–431. http://dx.doi.org/10.1038/gt.2009.144.
[20] A. Fischer, M. Cavazzana-Calvo, Gene therapy of inherited diseases, Lancet 371 (2008) 2044–2047. http://dx.doi.org/10.1016/S0140-6736(08)60874-0.
[21] S.Z. Guo, Q. Li, D.L. Bartlett, J.Y. Yang, B. Fang, Gene transfer: the challenge of regulated gene expression, Trends Mol. Med. 14 (2008) 410–418. http://dx.doi.org/10.1016/j.molmed.2008.07.003.
[22] D. Lee, K. Upadhye, P.N. Kumta, Nano-sized calcium phosphate (CaP) carriers for non-viral gene delivery, Mater. Sci. Eng. 177 (2012) 289–302. http://dx.doi.org/10.1016/j.mseb.2011.11.001.
[23] M.C. Woodle, P. Scaria, Cationic liposomes and nucleic acids, Curr. Opin. Colloid Interface Sci. 6 (2001) 78–84. http://dx.doi.org/10.1016/s1359-0294(00)00091-1.
[24] Y. Fedorov, A. King, E. Anderson, J. Karpilow, D. Ilsley, W. Marshall, A. Khvorova, Different delivery methods-different expression profiles, Nat. Methods 2 (2005) http://dx.doi.org/10.1038/nmeth0405-241.
[25] T.H. Wu, T. Teslaa, M.A. Teitell, P.Y. Chiou, Photothermal nanoblade for patterned cell membrane cutting, Opt. Express 18 (2010) 23153–23160. http://dx.doi.org/10.1364/OE.18.023153.
[26] R.R. Sun, M.L. Noble, S.S. Sun, S. Song, C.H. Miao, Development of therapeutic microbubbles for enhancing ultrasound-mediated gene delivery, J. Control. Release 182 (2014) 111–120. http://dx.doi.org/10.1016/j.jconrel.2014.03.002.
[27] J.A. Wyber, J. Andrews, A. D'Emanuele, The use of sonication for the efficient delivery of plasmid DNA into cells, Pharm. Res. 14 (1997) 750–756.
[28] J.A. O'Brien, S.C.R. Lummis, Nano-biolistics: a method of biolistic transfection of cells and tissues using a gene gun with novel nanometer-sized projectiles, BMC Biotechnol. 11 (2011) http://dx.doi.org/10.1186/1472-6750-11-66.
[29] R.-Y. Huang, P.-H. Chiang, W.-C. Hsiao, C.-C. Chuang, C.-W. Chang, Redox-sensitive polymer/SPIO nanocomplexes for efficient magnetofection and MR imaging of human cancer cells, Langmuir 31 (2015) 6523–6531. http://dx.doi.org/10.1021/acs.langmuir.5b01208.
[30] A.I. Daud, R.C. DeConti, S. Andrews, P. Urbas, A.I. Riker, V.K. Sondak, P.N. Munster, D.M. Sullivan, K.E. Ugen, J.L. Messina, R. Heller, Phase I trial of interleukin-12 plasmid electroporation in patients with metastatic melanoma, J. Clin. Oncol. Off. J. Am. Soc. Clin. Oncol. 26 (2008) 5896–5903. http://dx.doi.org/10.1200/JCO.2007.15.6794.
[31] S. Li, Electroporation gene therapy: new developments in vivo and in vitro, Curr. Gene Ther. 4 (2004) 309–316.
[32] E. Neumann, M. Schaefer-Ridder, Y. Wang, P.H. Hofschneider, Gene transfer into mouse lyoma cells by electroporation in high electric fields, EMBO J. 1 (1978) 841–845.
[33] R. Heller, M. Jaroszeski, A. Atkin, D. Moradpour, R. Gilbert, J. Wands, C. Nicolau, In vivo gene electroinjection and expression in rat liver, FEBS Lett. 389 (1996) 225–228.
[34] L.M. Mir, Therapeutic perspectives of in vivo cell electropermeabilization, Bioelectrochem. 53 (2001) 1–10.
[35] M.P. Rols, C. Delteil, M. Golzio, J. Teissié, Control by ATP and ADP of voltage-induced mammalian-cell-membrane permeabilization, gene transfer and resulting expression, Eur. J. Biochem. 254 (1998) 382–388.
[36] A.V. Titomirov, S. Sukharev, E. Kistanova, In vivo electroporation and stable transformation of skin cells of newborn mice by plasmid DNA, Biochim. Biophys. Acta Gene Struct. Expr. 1088 (1991) 131–134.
[37] A. Silve, I. Leray, M. Leguèbe, C. Poignard, L.M. Mir, Cell membrane permeabilization by 12-ns electric pulses: not a purely dielectric, but a charge-dependent phenomenon, Bioelectrochem. (Amsterdam, Netherlands) 106 (2015) 369–378. http://dx.doi.org/10.1016/j.bioelechem.2015.06.002.
[38] W. Frey, J.A. White, R.O. Price, P.F. Blackmore, R.P. Joshi, R. Nuccitelli, S.J. Beebe, K.H. Schoenbach, J.F. Kolb, Plasma membrane voltage changes during nanosecond pulsed electric field exposure, Biophys. J. 90 (2006) 3608–3615. http://dx.doi.org/10.1529/biophysj.105.072777.
[39] J. Deng, K.H. Schoenbach, E.S. Buescher, P.S. Hair, P.M. Fox, S.J. Beebe, The effects of intense submicrosecond electrical pulses on cells, Biophys. J. 84 (2003) 2709–2714.
[40] J.-M. Escoffre, T. Portet, L. Wasungu, J. Teissié, D. Dean, M.-P. Rols, What is (still not) known of the mechanism by which electroporation mediates gene transfer and expression in cells and tissues, Mol. Biotechnol. 41 (2009) 286–295. http://dx.doi.org/10.1007/s12033-008-9121-0.
[41] J. Teissie, M. Golzio, M.P. Rols, Mechanisms of cell membrane electropermeabilization: a minireview of our present (lack of ?) knowledge, Biochim. Biophys. Acta 1724 (2005) 270–280. http://dx.doi.org/10.1016/j.bbagen.2005.05.006.
[42] B. Ferraro, L.C. Heller, Y.L. Cruz, S. Guo, A. Donate, R. Heller, Evaluation of delivery conditions for cutaneous plasmid electrotransfer using a multielectrode array, Gene Ther. 18 (2011) 496–500. http://dx.doi.org/10.1038/gt.2010.171.
[43] L.C. Heller, M.J. Jaroszeski, D. Coppola, A.N. McCray, J. Hickey, R. Heller, Optimization of cutaneous electrically mediated plasmid DNA delivery using novel electrode, Gene Ther. 14 (2007) 275–280. http://dx.doi.org/10.1038/sj.gt.3302867.
[44] J.A. Weaver, Y. Chizmadzhev, Theory of electroporation: a review, Bioelectrochem. Bioenerg. 41 (1996) 135–160. http://dx.doi.org/10.1016/S0302-4598(96)05062-3.
[45] M. Naumowicz, A.Z. Figaszewski, Pore formation in lipid bilayer membranes made of phosphatidylcholine and cholesterol followed by means of constant current, Cell Biochem. Biophys. 66 (2013) 109–119. http://dx.doi.org/10.1007/s12013-012-9459-6.
[46] U. Pliquett, R.P. Joshi, V. Sridhara, K.H. Schoenbach, High electrical field effects on cell membranes, Bioelectrochem. (Amsterdam, Netherlands) 70 (2007) 275–282. http://dx.doi.org/10.1016/j.bioelechem.2006.10.004.
[47] A. Ivorra, B. Rubinsky, In vivo electrical impedance measurements during and after electroporation of rat liver, Bioelectrochem. 70 (2007) 287–295.
[48] M. Pavlin, D. Miklavcic, Theoretical and experimental analysis of conductivity, ion diffusion and molecular transport during cell electroporation-relation between short-lived and long-lived pores, Bioelectrochem. (Amsterdam, Netherlands) 74 (2008) 38–46. http://dx.doi.org/10.1016/j.bioelechem.2008.04.016.
[49] A. Ivorra, B. Al-Sakere, B. Rubinsky, L.M. Mir, In vivo electrical conductivity measurements during and after tumor electroporation: conductivity changes reflect the treatment outcome, Phys. Med. Biol. 54 (2009) 5949–5963. http://dx.doi.org/10.1088/0031-9155/54/19/019.
[50] M. Leguèbe, A. Silve, L.M. Mir, C. Poignard, Conducting and permeable states of cell membrane submitted to high voltage pulses: mathematical and numerical studies validated by the experiments, J. Theor. Biol. 360 (2014) 83–94. http://dx.doi.org/10.1016/j.jtbi.2014.06.027.
[51] F. Clemente, P. Arpaia, C. Manna, Characterization of human skin impedance after electrical treatment for transdermal drug delivery, Measur. 46 (2013) 3494–3501. http://dx.doi.org/10.1016/j.measurement.2013.06.033.
[52] T. García-Sánchez, M. Guitart, J. Rosell-Ferrer, A.M. Gómez-Foix, R. Bragós, A new spiral microelectrode assembly for electroporation and impedance measurements of adherent cell monolayers, Biomedical Microdevices 16 (2014) 575–590. http://dx.doi.org/10.1007/s10544-014-9860-6.
[53] S.-L. Tsai, M.-H. Wang, 24 h observation of a single HeLa cell by impedance measurement and numerical modeling, Sensors Actuators B Chem. (2016) http://dx.doi.org/10.1016/j.snb.2016.01.107.
[54] T. García-Sánchez, A. Azan, I. Leray, J. Rosell-Ferrer, R. Bragós, L.M. Mir, Interpulse multifrequency electrical impedance measurements during electroporation of adherent differentiated myotubes, Bioelectrochem. 105 (2015) 123–135. http://dx.doi.org/10.1016/j.bioelechem.2015.05.018.